Supporting Information for:

Chemical additives enable native mass spectrometry measurement of membrane protein oligomeric state within intact nanodiscs

James E. Keener,[1] Dane Evan Zambrano,[1] Guozhi Zhang,[1] Ciara K. Zak,[1] Deseree J. Reid,[1] Bhushan S. Deodhar,[1] Jeanne E. Pemberton,[1] James S. Prell,[2] Michael T. Marty[1,*]

[1]Department of Chemistry and Biochemistry, University of Arizona, Tucson, AZ 85721 USA

[2]Department of Chemistry and Biochemistry, University of Oregon, Eugene, OR 97403 USA

*Email: mtmarty@email.arizona.edu

SUPPLEMENTAL METHODS

Protein Sample Preparation

Stock myoglobin solutions were prepared by dissolving myoglobin in 0.2 M ammonium acetate at 3 mg/mL. Samples were then buffer exchanged into 0.2 M ammonium acetate using Micro Bio-Spin Columns (Bio-Rad Laboratories Inc). AmtB and AqpZ in detergent were prepared by adding TEV protease to the purified proteins to remove the MBP or GFP tags, respectively. Clipped proteins were purified by IMAC and buffer exchanged into either 1% OG or 0.5% C8E4 (Anatrace) detergent with 0.2 M ammonium acetate at pH 6.8 using a Superdex 200 Increase 5/150 SEC column (GE Healthcare). Proteins in detergent were concentrated to 1–10 μM using a 100 kDa molecular weight cut-off concentrator (EMD Millipore).

Thermal Stability Measurements

Thermal stability measurements were performed using a NanoTemper Tycho NT.6 nano-differential scanning fluorimetry (nanoDSF) instrument. Membrane proteins solubilized in nanodiscs or detergents were diluted 1:6 or 1:5 v/v, respectively, to minimize sample consumption. Samples were prepared in the same way as for native MS as described in the Methods section and were loaded onto Tycho NT.6 Capillaries (NanoTemper Technologies). The temperature was ramped from 35–95 °C over 3 minutes, and the ratio of tryptophan fluorescence at 350 and 330 nm was monitored. Changes in the fluorescence ratio as a function of temperature were plotted and inflection points were detected using vendor software to determine the melting temperatures (T_m).

Surface Tension Measurements

Surface tension measurements were performed using the du Noüy ring method with a Biolin Scientific force tensiometer, model Sigma 701 employing a Pt:Ir ring. Aqueous solutions of PC and GC were prepared by dissolution in ultrapure Millipore water (18 M, <6 ppb TOC) and 0.2 M ammonium acetate. These solutions were sonicated for 6 h in glass vials and allowed to equilibrate overnight at ambient temperature before measurements were initiated. Water purity was confirmed by verifying a surface tension (γ) of 71–72 mN/m. Before each measurement, the Pt:Ir ring was rinsed with methanol and acetone and allowed to air dry. Three replicate measurements were averaged for each sample solution (<0.5 mN/m deviation indicating equilibrium), and three independently-prepared solutions were measured for both PC and GC.

Chemical Modeling and Gas-Phase Basicity Computations

Computational modeling was performed using the University of Oregon's High-Performance Computing Cluster, Talapas. Trial structures for neutral and protonated forms of supercharging reagents were generated in the molecular modeling program Avogadro v. 1.2.0. Initial structures were subjected to a weighted rotor search using the MMFF94 force field, and low-energy structures representing protonation at each basic site were geometry optimized in Gaussian 9.0 (Gaussian, Inc.) at the B3LYP/6-31G* or MP2/6-31G* level of theory. The resulting structures were further geometry optimized at the B3LYP/6-31++G** or MP2/6-31++G** level of theory, and harmonic vibrational frequencies were calculated at the same level of theory. Zero-point corrected electronic energies, enthalpies, and Gibbs free energies at 298.15 K were computed without rescaling of vibrational frequencies. Proton affinity (respectively, gas-phase basicity) values were computed as described previously.[1] Briefly, the enthalpy (resp., Gibbs free energy) of the lowest-energy protonated form of the supercharging reagent was subtracted from that of the neutral form and corrected for the enthalpy, 6.2 kJ/mol (resp., Gibbs free energy, −26.3 kJ/mol)[2], of a gas of protons at standard temperature and

pressure. When applied to water, this procedure yielded a computed proton affinity of 691 (resp., 693) kJ/mol at the B3LYP/6-31++G** (resp., MP2/6-31++G**) and a gas-phase basicity of 659 (resp., 662) kJ/mol, in excellent agreement with the experimental values reported by Hunter and Lias[3] (691 and 660 kJ/mol).

SUPPLEMENTAL DISCUSSION

Thermal Stability Analysis

Supercharging is thought to result from chemical and/or thermal denaturing in the late stages of the ESI droplet.[4] Thus, we hypothesized that the stability of nanodisc ions produced in the presence of supercharging reagents might correlate with solution-phase thermal stability in the presence of the same reagents. To test this hypothesis, we performed nano-differential scanning fluorimetry (DSF). DSF monitors differences in the fluorescence of tryptophan residues as they are exposed to solvent due to unfolding at increased temperatures. We tested empty POPC nanodiscs as well as AmtB and AqpZ nanodiscs. We also tested AmtB and AqpZ in OG and C8E4 micelles to examine the effects of the nanodisc on the membrane protein stability. Finally, we tested myoglobin as a small soluble protein standard to compare the trends (Figure S-10A). However, AmtB in nanodiscs and OG did not show clear melting transitions, consistent with either a very broad transition or high stability that prevents unfolding below the instrument maximum of 95 °C. Furthermore, two transitions were observed for AqpZ in C8E4, preventing confident interpretation of the stability.

Several clear trends emerge from the thermal stability measurements. The melting temperatures across myoglobin, membrane proteins in detergent, empty nanodiscs, and AqpZ in nanodiscs show the following trend: PC ≈ 4V < GC < No additive ≈ IM (Figure S-10A and Table S-2). The lower thermal stability in supercharging reagents supports the hypothesis that thermal and/or chemical unfolding in the ESI droplet may cause supercharging.[4] Although the differences between GC and PC are opposite the expected trend (GC is less thermally destabilizing in solution compared to PC but generally more supercharging during ESI), the precise temperature and solvent concentration may be different in the ESI droplet, which could modulate these ESI effects. Because these supercharging reagents are less volatile than water and ammonium acetate, they likely concentrate in the electrospray droplet and raise its temperature before charge transfer to the analyte is complete.[4-7] In any case, solution-phase thermal stability does not completely explain the stability differences between empty nanodiscs and membrane protein nanodiscs and between the results observed in positive and negative ionization mode. Thus, thermal stability likely provides some basis for charging and stabilization during ESI, but it is not a complete explanation.

Surface Tension Analysis

The charge residue model of ESI predicts that the charge of a protein ion is dependent on the Rayleigh limit, which is proportional to the square root of the droplet surface tension.[8,9] Changes in surface tension caused by supercharging reagents were proposed to explain some of the earliest data on supercharging,[10] but observation of supercharging at lower surface tensions have questioned the surface tension explanation.[11,12] Literature values for the bulk surface tension of neat PC (41 mN/m), 4V (40 mN/m),[13] and GC (44 mN/m)[14] are all lower than that of water (72 mN/m) (Table S-3). Thus, bulk surface tension values alone would predict lower charges from these supercharging reagents compared with no additive.

Because significant differences were previously observed in supercharging between pure water and ammonium acetate solution,[14] we measured the bulk surface tension of PC and GC mixed with either water or 0.2 M ammonium acetate solution. Ammonium acetate solution had a very similar surface tension to pure water, and addition of either 5% PC or GC lowered the surface tension substantially in both solutions (Figure S-10B). Although PC showed similar surface tension in both water and aqueous ammonium acetate solution, GC showed significant differences. The unexpectedly higher surface tension of GC in water correlates with differences in supercharging between water and ammonium acetate solution previously observed by Williams and coworkers.[14] However, differences in supercharging between water and ammonium acetate solution were also previously observed with PC, for which only minor differences in bulk surface tension were measured. Ultimately, the similarity in surface tension between GC and PC in ammonium acetate solution reveal surface tension alone does not explain the supercharging data.

Consideration of Other Physical Properties

To help understand the differences between reagents, we examined differences in physical constants beyond the surface tension (Table S-3). The dipole moment is very similar between carbonate reagents, so it is unlikely to be a significant factor explaining their different supercharging behavior.[15] Moreover, the gas-phase basicity and proton affinity are similar between the carbonates, so proton transfer reactions between neutral solvent molecules and the charged complex are unlikely in positive mode, which is similar to other supercharging reagents.[1] Intriguingly, both B3LYP and MP2 computations indicate that, while the carbonyl oxygen is the preferred site of protonation for all three carbonates in the gas phase and results in a stable protonated ion, protonation at either of the other carbonate oxygen atoms leads to immediate loss of a carbon dioxide molecule from the carbonate ion. The potential significance of this chemical reactivity of cyclic carbonate supercharging reagents in the gas phase is unknown but warrants future investigation.

Two additional physical properties that are significantly different between PC and GC are the boiling point and the dielectric constant. The higher boiling point of GC may explain why it is generally a more effective supercharging reagent. Because GC has a higher boiling point, it may achieve higher droplet temperatures and thus greater thermal destabilization.[4] However, boiling point differences do not explain the observed differences between positive and negative ionization mode. The dielectric constant of the

solvent can influence ESI charging by influencing its ability to solvate charge.[16,17] Changes in pK_a and pK_b due to differences in dielectric between PC and GC may describe some of the differential behavior in positive and negative mode, but prior work by Donald and coworkers[18] has shown poor correlation between the extent of supercharging and dielectric constant in denatured proteins. Thus, a simple explanation based on physical constants is unable to fully rationalize the effects of supercharging reagents on biomolecular complexes.[18]

SUPPLEMENTAL FIGURES

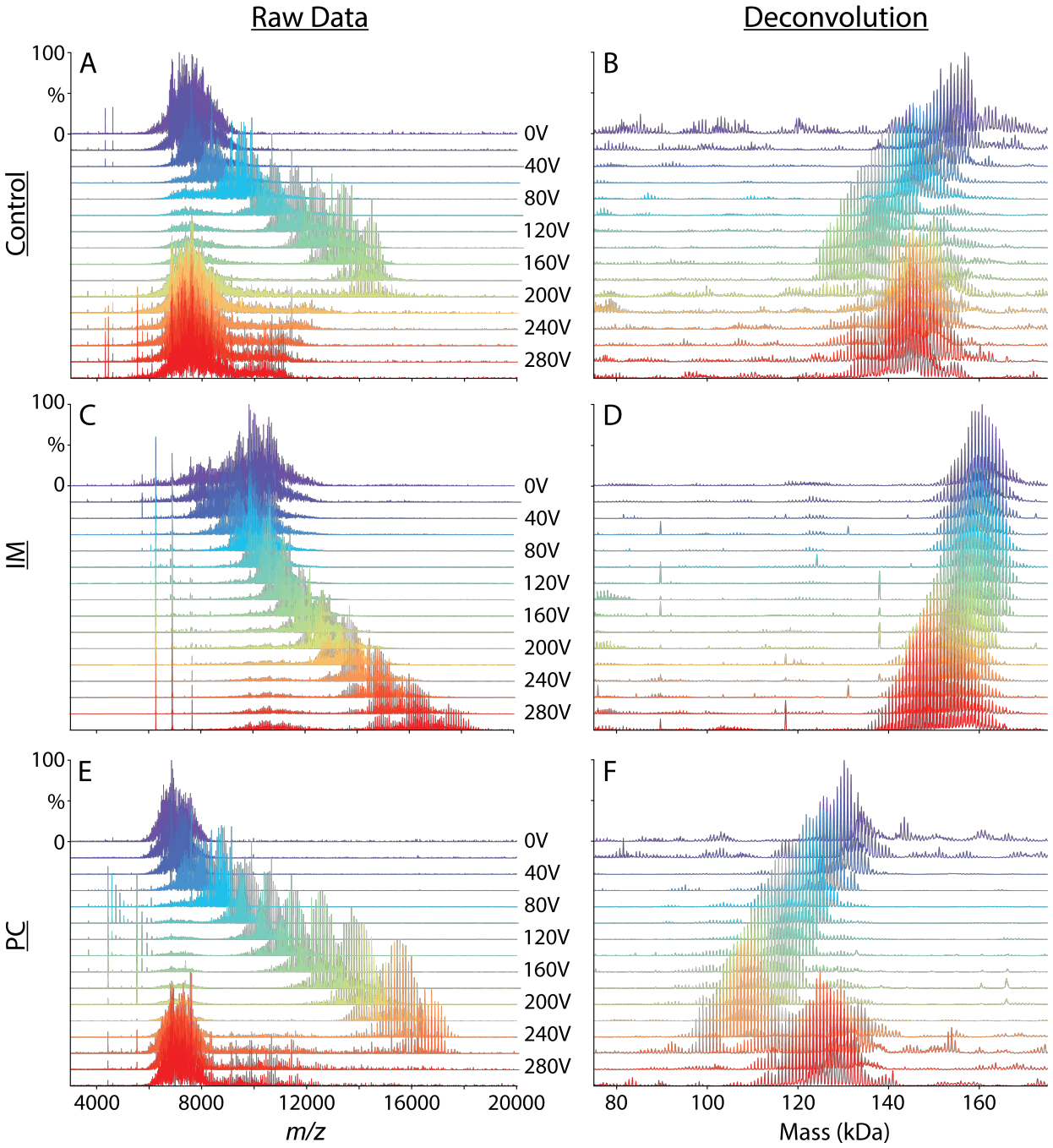

Figure S-1. Representative positive ion mode mass spectra (A, C, E) and zero-charge deconvolved spectra (B, D, F) of empty POPC nanodiscs with no additive (A and B), 40 mM IM (C and D), or 5% PC (E and F). Spectra are shown at increasing collision voltages from 0 V (purple) to 300 V (red) in 20 V increments applied using the in-source trapping region. Note: imperfect trapping is sometimes observed at higher collision voltages, leading to ions not being fully activated. We thus limited our analysis to 0–160 V for average mass analysis shown in Figure 3.

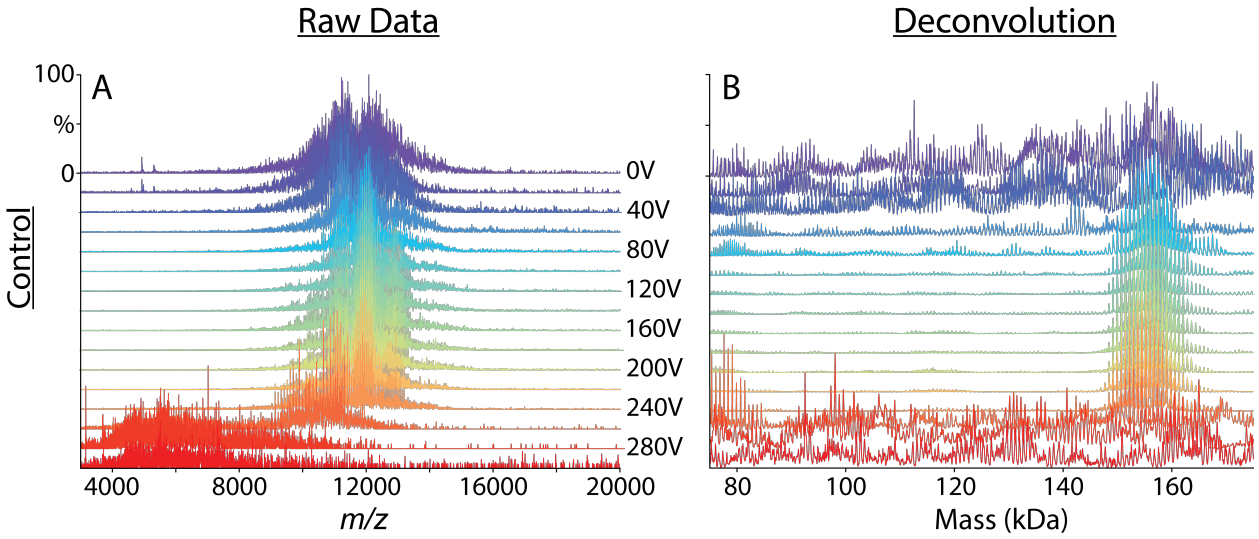

Figure S-2. Representative negative ion mode mass spectra (A) and zero-charge deconvolved spectra (B) of empty POPC nanodiscs. Collision voltage was applied from 0 V (purple) to 300 V (red) increasing in 20 V increments using the in-source trapping region.

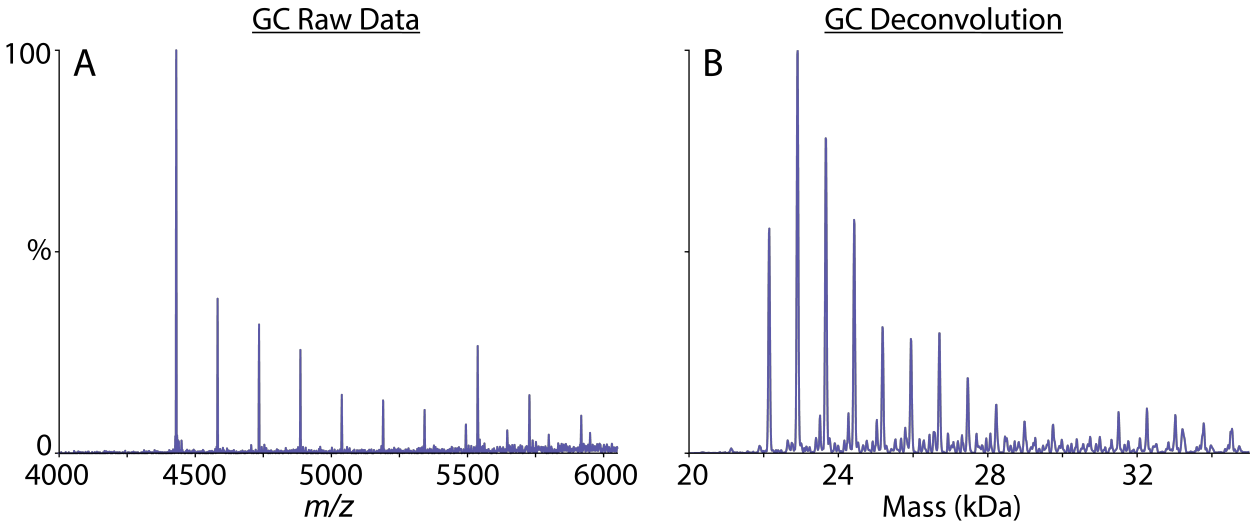

Figure S-3. The positive ionization mode mass spectrum (A) and zero-charge deconvolved spectrum (B) of empty POPC nanodiscs with 5% glycerol carbonate at a low collision voltage (20 V). Only free MSP with a small amount of bound lipid are observed.

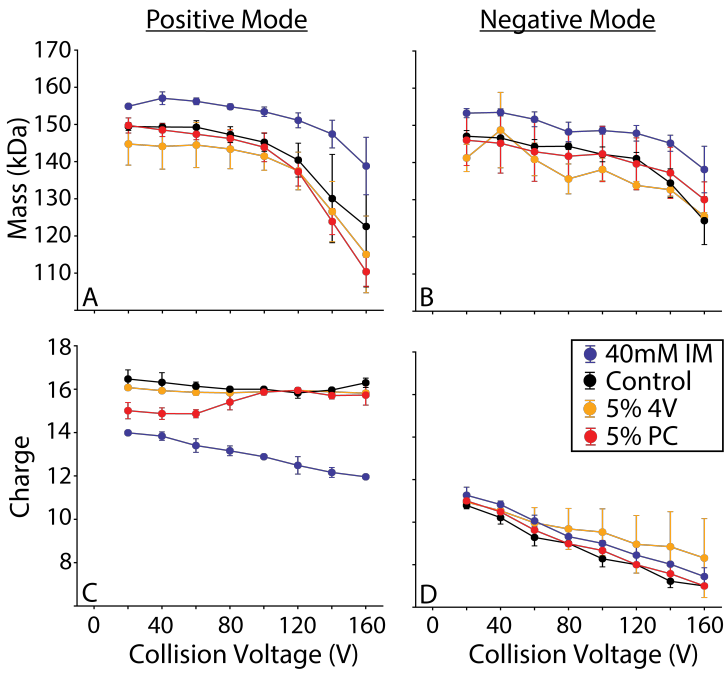

Figure S-4. The average mass (A, B) and charge (C, D) versus collision voltage for empty POPG nanodiscs with 40 mM IM (*blue*), no additive (*black*), 5% 4V (*orange*), and 5% PC (*red*) in both positive (A, C) and negative (B, D) ionization modes. Error bars show the standard deviation of three replicate nanodisc assemblies.

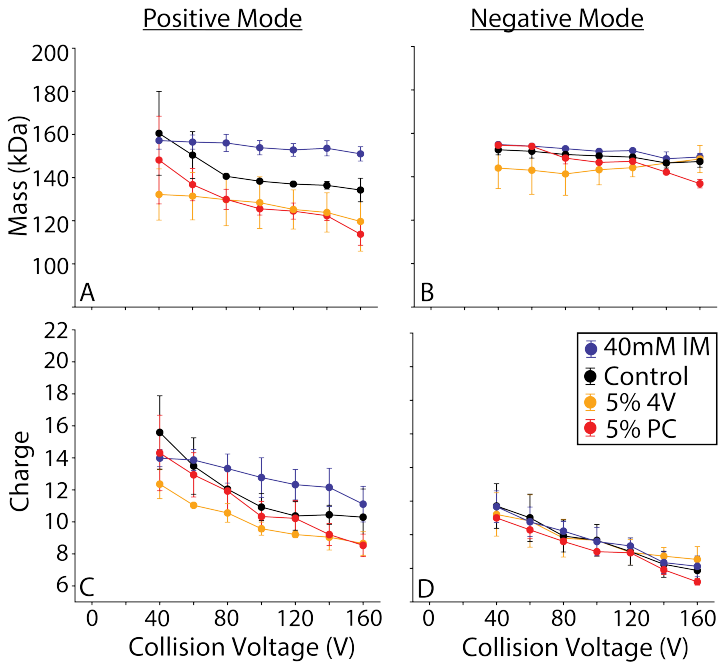

Figure S-5. The average mass (A, B) and charge (C, D) versus collision voltage for empty nanodisc with 50/50 POPG/POPC with 40 mM IM (*blue*), no additive (*black*), 5% 4V (*orange*), and 5% PC (*red*) in both positive (A, C) and negative (B, D) ionization modes. Error bars show the standard deviation of three replicate nanodisc assemblies.

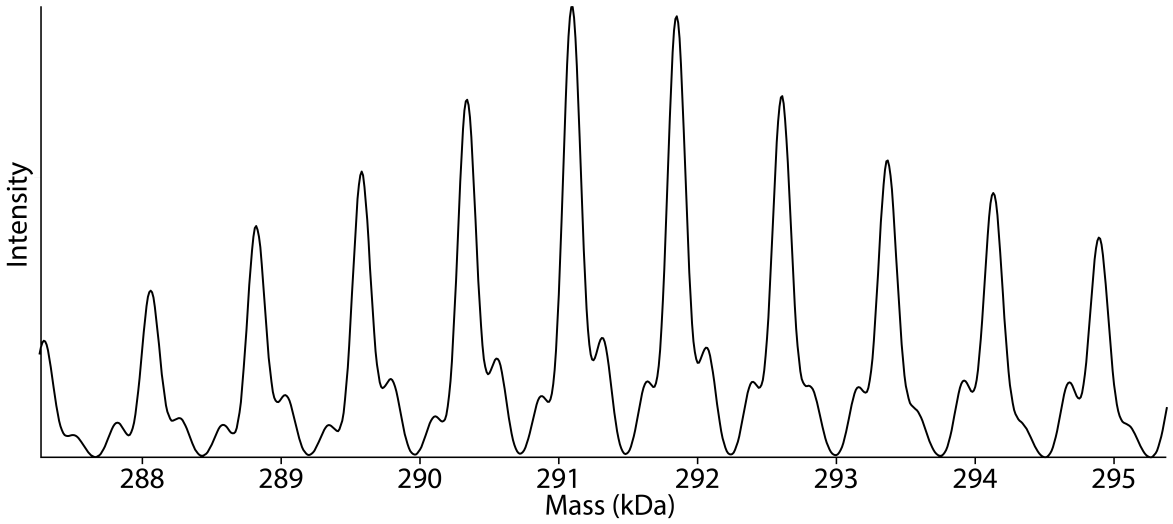

Figure S-6. Example deconvolved mass distribution of AmtB nanodiscs with added 4V in negative ion mode summed from 0–300 V. Data from Figure 4I is magnified to show triplet peaks, which indicate two MSP molecules present in the complex.

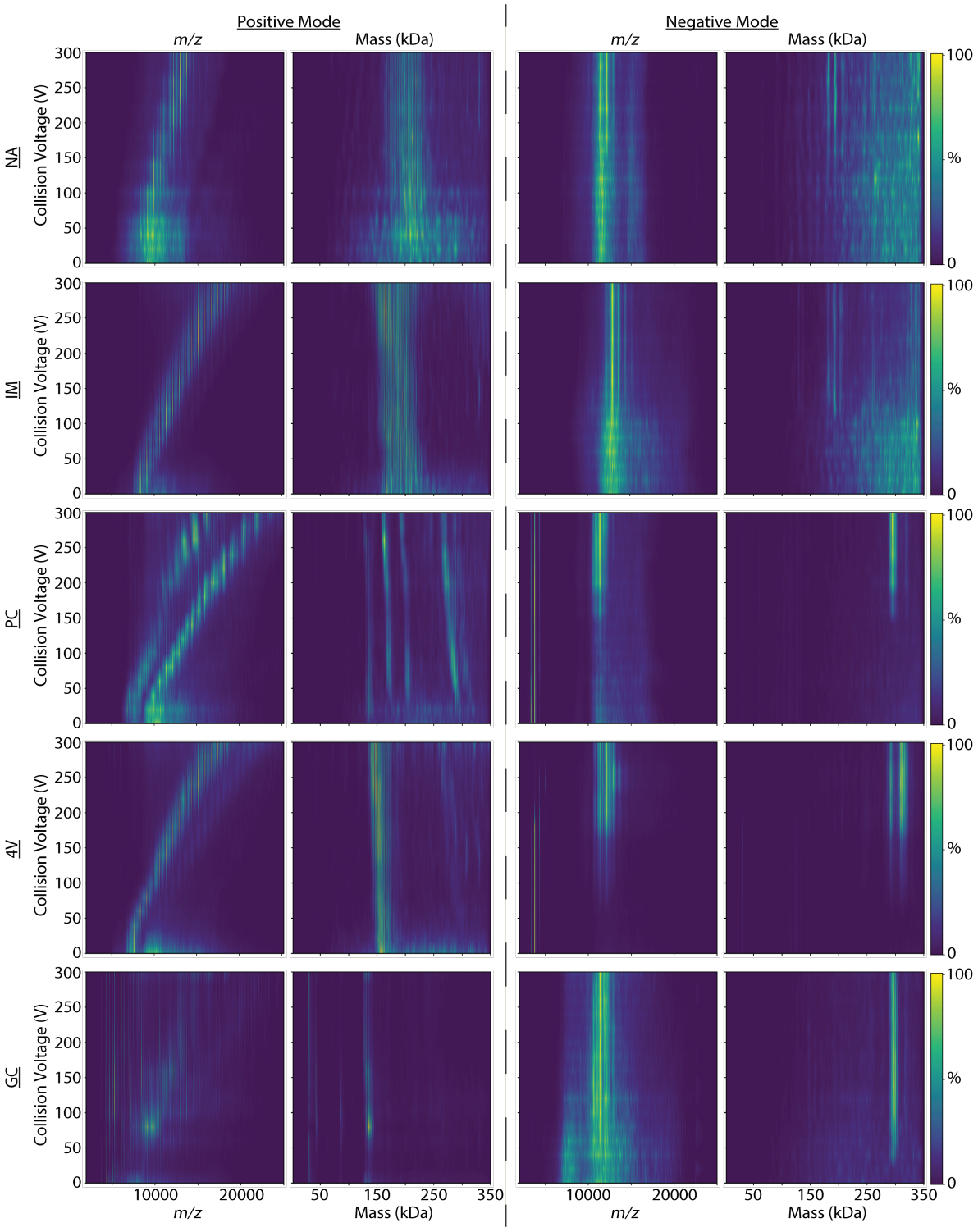

Figure S-7. Representative mass spectra and deconvolved mass distributions of AmtB nanodiscs in the presence of different charge manipulation reagents in positive (*left*) and negative (*right*) ionization modes at increasing levels of collisional activation.

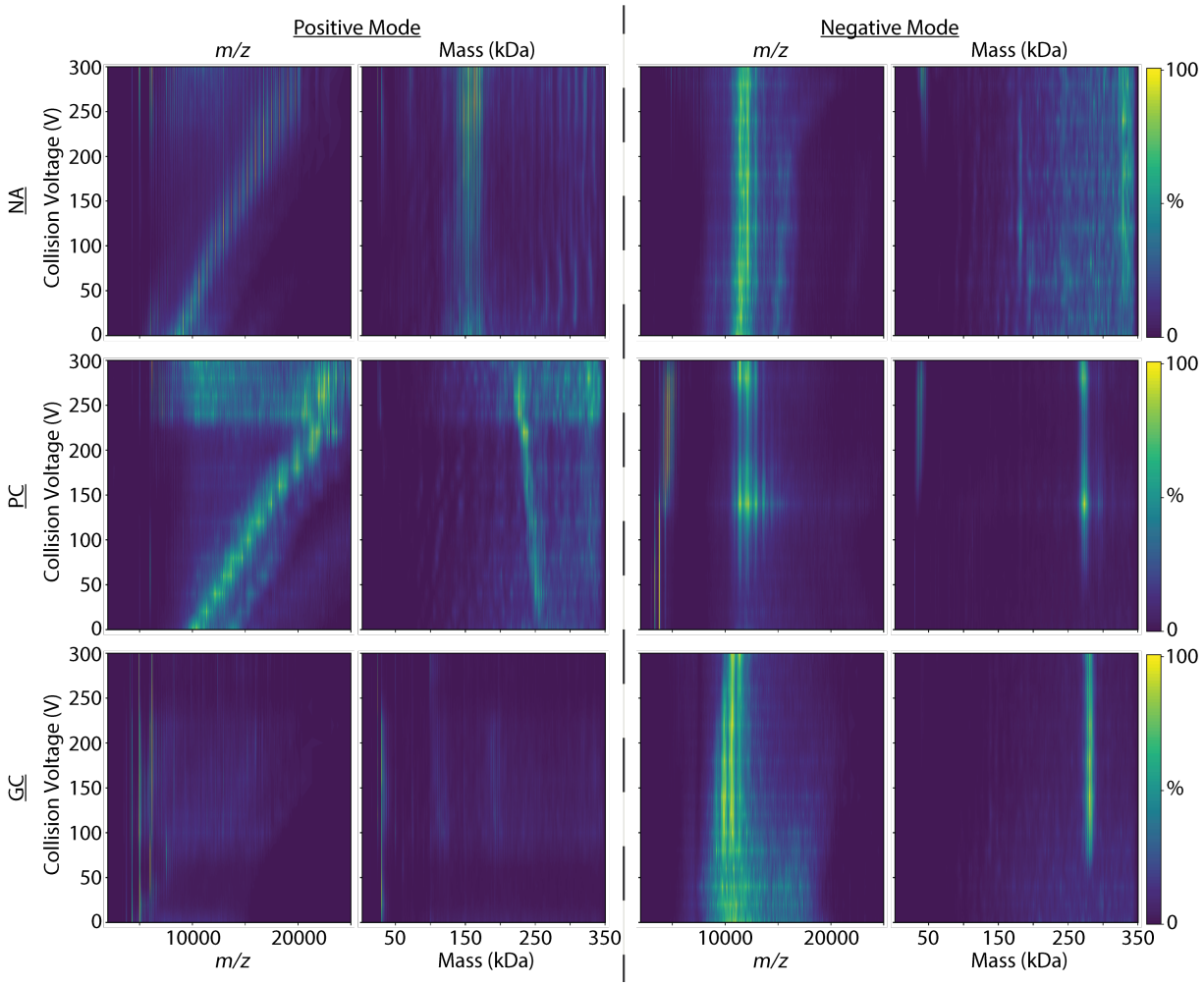

Figure S-8. Representative mass spectra and deconvolved mass distributions of AqpZ nanodiscs in the presence of different charge manipulation reagents in positive (*left*) and negative (*right*) ionization modes at increasing levels of collisional activation.

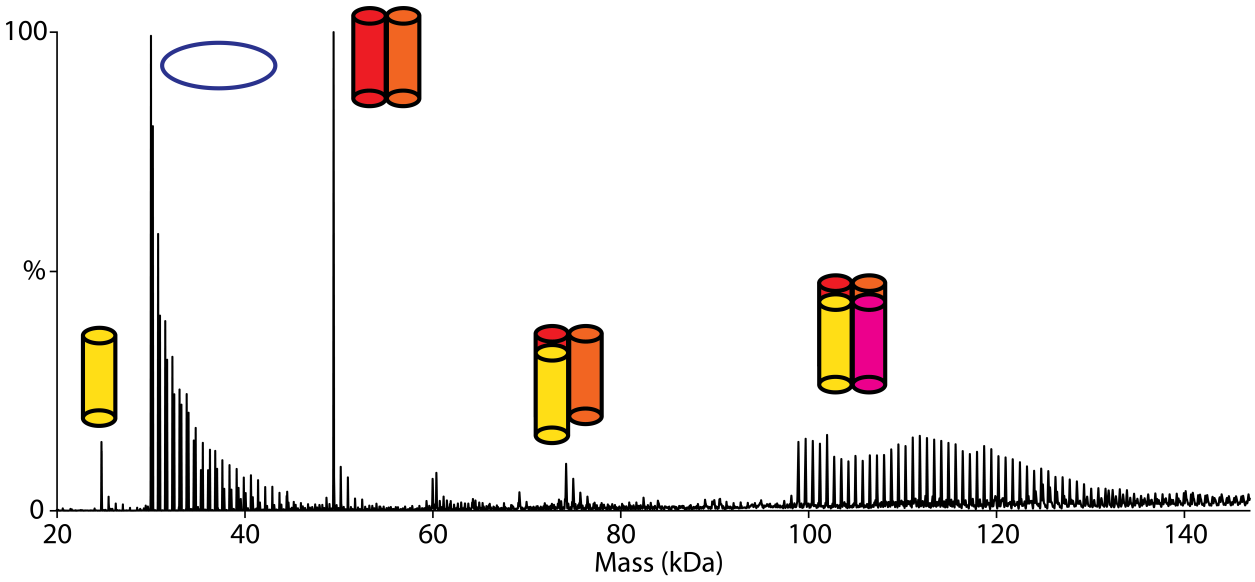

Figure S-9. Example deconvolved mass distribution of AqpZ nanodiscs with added GC in positive ion mode summed from 0–300 V showing the low mass species of free MSP (with a doublet peak), intact AqpZ tetramer, and AqpZ monomer, dimer, and trimer fragments.

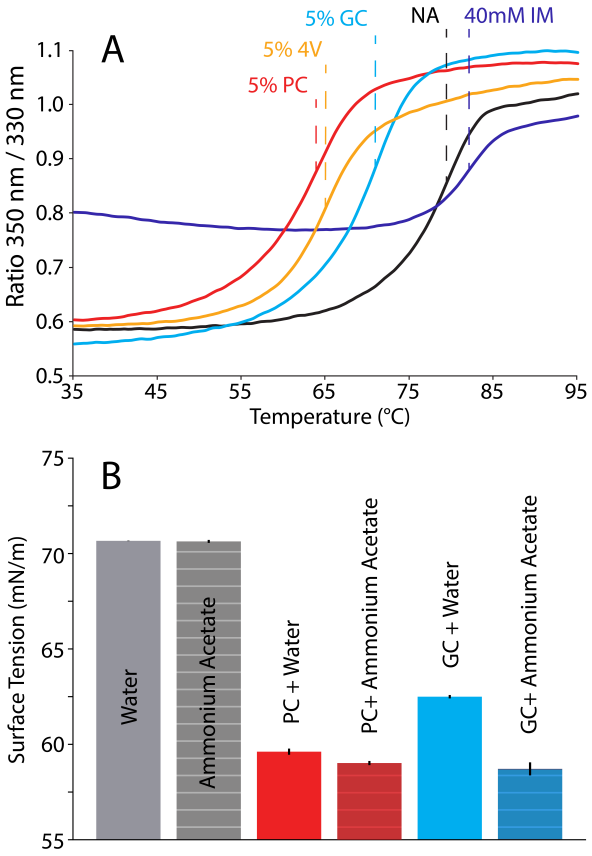

Figure S-10. Representative nanoDSF thermal unfolding data for myoglobin with either no additive (NA) or different charge manipulation reagents (A) and the surface tension of solutions of water and 0.2 M ammonium acetate with either no additive, 5% PC, or 5% GC (B). Melting temperatures from (A) are provided in Table S-2.

SUPPLEMENTAL TABLES

	Sample	Supercharging						Charge Reducing	
Reagent		PC	4V	GC	PC	4V	GC	IM	IM
Polarity		+	+	+	-	-	-	+	-
Lipids	POPC ND	D	D	D	D	N		S	N
	PC/PG ND	D	D		N	N		S	N
	POPG ND	N	N		N	N		S	S
	AmtB ND	S/D	S/D	D	S	S	S	N	
	AqpZ ND	S		D	S		S		
MSP	POPC ND	N	N	D	N	N		N	N
	PC/PG ND	N	N		N	N		N	N
	POPG ND	N	N		N	N		N	N
	AmtB ND	N/S	N/S	D	S	S	S	N	
	AqpZ ND	S		D	S		S		

Table S-1. Summary of the effects of different charge manipulation reagents on dissociation of lipids (*top*) and MSP (*bottom*) from nanodiscs in different ionization polarities. Stabilities compared to controls with no additives are annotated with S = stabilized (*green*), N = no effect (*white*), and D = destabilized (*red*). Black squares mark data that was either not collected or uninterpretable. Nanodisc samples correspond to empty MSP1D1(-) and either POPC, POPC/POPG, or POPG and MSP1E3D1(-)/MSP1E3D1T2(-) POPC nanodiscs with either AmtB or AqpZ.

Sample	PC T_m (°C)	4V T_m (°C)	GC T_m (°C)	NA T_m (°C)	IM T_m (°C)
POPC ND	78.5 ± 5.3	78.2 ± 2.2	> 95	> 95	> 95
AqpZ ND	82.9 ± 1.5	80.1 ± 3.7	93.5 ± 2.7	> 95	> 95
AmtB C8E4	66.4 ± 0.2	NM	75.0 ± 0.2	74.7 ± 1.5	76.0 ± 0.1
AqpZ OG	70.2 ± 1.3	NM	80.2 ± 0.9	83.0 ± 0.4	82.6 ± 0.1
Myoglobin	62.9 ± 0.4	64.3 ± 0.5	70.6 ± 0.2	77.8 ± 0.3	79.2 ± 0.3

Table S-2. Melting temperatures (T_m) for empty POPC MSP1D1(-) nanodiscs, AqpZ nanodiscs, AmtB in C8E4 micelles, AqpZ in OG micelles, and myoglobin measured by nanoDSF. The color gradient depicts the relative thermal stability, with green indicating the most stable conditions and red indicating the least stable. Non-miscible mixtures for which measurements were not performed are labelled "NM". Error bars show the standard deviation for triplicate sample preparations.

Constant	PC	4V	GC	Water	IM
Surface Tension (mN/m)	41[13]	40[13]	44[14]	72	ND
Dipole Moment (μ/D)	5.4[19]	5.6[13]	5.05[19]	1.85[20]	3.84[20]
Boiling Point (°C)	242[20]	237[v]	354[14]	100[20]	257[20]
Dielectric Constant at 25 °C	65.5[19]	ND	109.7[19]	78.4[20]	ND
Gas-Phase Basicity (kJ/mol) B3LYP/6-31++G**	797	801	790	660[3]	909[3]
Gas-Phase Basicity (kJ/mol) MP2/6-31++G**	785	789	778	660[3]	909[3]
Proton Affinity (kJ/mol) B3LYP/6-31++G**	828	833	821	691[3]	943[3]
Proton Affinity (kJ/mol) MP2/6-31++G**	817	820	808	691[3]	943[3]

Table S-3. Table of physical constants for charge manipulation reagents and water. "ND" indicates the values were not determined. Literature values are referenced with superscripts and correspond to references below. [v] indicates the value was obtained from the vendor. All other values were measured or calculated. The calculated gas-phase basicity and proton affinities are listed separately for the B3LYP/6-31++G** and MP2/6-31++G** methods. Note: the literature value for gas-phase basicity and proton affinity for imidazole and water were determined experimentally, and the same values are listed twice for reference.

SUPPLEMENTAL REFERENCES

(1) Sterling, H.J.; Prell, J.S.; Cassou, C.A.; Williams, E.R. *J. Am. Soc. Mass. Spectrom.* **2011**, *22*, 1178-1186.
(2) Fifen, J.J.; Dhaouadi, Z.; Nsangou, M. *J. Phys. Chem. A* **2014**, *118*, 11090-11097.
(3) Hunter, E.P.L.; Lias, S.G. *J. Phys. Chem. Ref. Data* **1998**, *27*, 413-656.
(4) Donor, M.T.; Ewing, S.A.; Zenaidee, M.A.; Donald, W.A.; Prell, J.S. *Anal. Chem.* **2017**, *89*, 5107-5114.
(5) Metwally, H.; McAllister, R.G.; Popa, V.; Konermann, L. *Anal. Chem.* **2016**, *88*, 5345-5354.
(6) Hogan, C.J., Jr.; Ogorzalek Loo, R.R.; Loo, J.A.; de la Mora, J.F. *Phys. Chem. Chem. Phys.* **2010**, *12*, 13476-13483.
(7) Sterling, H.J.; Daly, M.P.; Feld, G.K.; Thoren, K.L.; Kintzer, A.F.; Krantz, B.A.; Williams, E.R. *J. Am. Soc. Mass. Spectrom.* **2010**, *21*, 1762-1774.
(8) Wilm, M. *Mol. Cell. Proteomics* **2011**, *10*, M111 009407.
(9) Konermann, L.; Ahadi, E.; Rodriguez, A.D.; Vahidi, S. *Anal. Chem.* **2013**, *85*, 2-9.
(10) Iavarone, A.T.; Williams, E.R. *J. Am. Chem. Soc.* **2003**, *125*, 2319-2327.
(11) Šamalikova, M.; Grandori, R. *J. Am. Chem. Soc.* **2003**, *125*, 13352-13353.
(12) Loo, R.R.O.; Lakshmanan, R.; Loo, J.A. *J. Am. Soc. Mass. Spectrom.* **2014**, *25*, 1675-1693.
(13) Zenaidee, M.A.; Donald, W.A. *Analyst* **2015**, *140*, 1894-1905.
(14) Going, C.C.; Xia, Z.; Williams, E.R. *Analyst* **2015**, *140*, 7184-7194.
(15) Douglass, K.A.; Venter, A.R. *J. Am. Soc. Mass Spectrom.* **2012**, *23*, 489-497.
(16) Cole, R.B.; Harrata, A.K. *J. Am. Soc. Mass. Spectrom.* **1993**, *4*, 546-556.
(17) Wang, G.; Colecor, R.B. *J. Am. Soc. Mass. Spectrom.* **1996**, *7*, 1050-1058.
(18) Teo, C.A.; Donald, W.A. *Anal. Chem.* **2014**, *86*, 4455-4462.
(19) Chernyak, Y. *Journal of Chemical & Engineering Data* **2006**, *51*, 416-418.
(20) Rumble, J.R.; Lide, D.R.; Bruno, T.J.: *CRC Handbook of Chemistry and Physics*; 99th edition ed.; CRC Press: Boca Raton, 2018.